Cosmic ray shower rate variations detected by the ARGO-YBJ experiment during thunderstorms

Axikegu,[1] B. Bartoli,[2,3] P. Bernardini,[4,5] X. J. Bi,[6,7,8] Z. Cao,[6,7,8] S. Catalanotti,[2,3] S. Z. Chen,[6,7] T. L. Chen,[9] S. W. Cui,[10] B. Z. Dai,[11] A. D'Amone,[4,5] Danzengluobu,[9] I. De Mitri,[12,13] B. D. D'Ettorre Piazzoli,[2,14] T. Di Girolamo,[2,3] G. Di Sciascio,[14] C. F. Feng,[15] Zhenyong Feng,[1] W. Gao,[15] Q. B. Gou,[6,7] Y. Q. Guo,[6,7] H. H. He,[6,7,8] Haibing Hu,[9] Hongbo Hu,[6,7,8] M. Iacovacci,[2,3] R. Iuppa,[16,17] H. Y. Jia,[1] Labaciren,[9] H. J. Li,[9] C. Liu,[6,7] J. Liu,[11] M. Y. Liu,[9] H. Lu,[6] L. L. Ma,[6,7] X. H. Ma,[6,7] G. Mancarella,[4,5] S. M. Mari,[18,19] G. Marsella,[4,5] S. Mastroianni,[3] P. Montini,[20] C. C. Ning,[9] L. Perrone,[4,5] P. Pistilli,[18,19] P. Salvini,[21] R. Santonico,[14,22] P. R. Shen,[6] X. D. Sheng,[6,7] F. Shi,[6] A. Surdo,[5] Y. H. Tan,[6] P. Vallania,[23,24] S. Vernetto,[22,23] C. Vigorito,[24,25] H. Wang,[6] C. Y. Wu,[6,7] H. R. Wu,[6,7] L. Xue,[15] Q. Y. Yang,[11] X. C. Yang,[11] Z. G. Yao,[6,7] A. F. Yuan,[9] M. Zha,[6,7] H. M. Zhang,[6] L. Zhang,[11] X. Y. Zhang,[15] Y. Zhang,[6,7] J. Zhao,[6,7] Zhaxiciren,[9] Zhaxisangzhu,[9] X. X. Zhou,[1,*] F. R. Zhu,[1] and Q. Q. Zhu[6]

(ARGO-YBJ Collaboration)

[1]*School of Physical Science and Technology, Southwest Jiaotong University, 610031 Chengdu, Sichuan, China*
[2]*Dipartimento di Fisica dell'Università di Napoli "Federico II," Complesso Universitario di Monte Sant'Angelo, via Cinthia, I-80126 Napoli, Italy*
[3]*Istituto Nazionale di Fisica Nucleare, Sezione di Napoli, Complesso Universitario di Monte Sant'Angelo, via Cinthia, I-80126 Napoli, Italy*
[4]*Dipartimento Matematica e Fisica "Ennio De Giorgi," Università del Salento, via per Arnesano, I-73100 Lecce, Italy*
[5]*Istituto Nazionale di Fisica Nucleare, Sezione di Lecce, via per Arnesano, I-73100 Lecce, Italy*
[6]*Key Laboratory of Particle Astrophysics, Institute of High Energy Physics, Chinese Academy of Sciences, 100049 Beijing, China*
[7]*TIANFU Cosmic Ray Research Center, 610095 Chengdu, Sichuan, China*
[8]*University of Chinese Academy of Sciences, 100049 Beijing, China*
[9]*Key Laboratory of Cosmic Rays (Tibet University), Ministry of Education, 850000 Lhasa, Tibet, China*
[10]*Hebei Normal University, 050024 Shijiazhuang, Hebei, China*
[11]*School of Physics and Astronomy, Yunnan University, 650091 Kunming, Yunnan, China*
[12]*Gran Sasso Science Institute (GSSI), Via Iacobucci 2, L'Aquila, Italy*
[13]*INFN Laboratori Nazionali del Gran Sasso, Via Acitelli, Assergi, L'Aquila, Italy*
[14]*Istituto Nazionale di Fisica Nucleare, Sezione di Roma Tor Vergata, via della Ricerca Scientifica 1, I-00133 Roma, Italy*
[15]*Institute of Frontier and Interdisciplinary Science, Shandong University, 266237 Qingdao, Shandong, China*
[16]*Dipartimento di Fisica dell'Università di Trento, via Sommarive 14, 38123 Povo, Italy*
[17]*Trento Institute for Fundamental Physics and Applications, via Sommarive 14, 38123 Povo, Italy*
[18]*Dipartimento di Fisica dell'Università "Roma Tre", via della Vasca Navale 84, I-00146 Roma, Italy*
[19]*Istituto Nazionale di Fisica Nucleare, Sezione di Roma Tre, via della Vasca Navale 84, I-00146 Roma, Italy*
[20]*Dipartimento di Fisica dell'Università di Roma "La Sapienza" and INFN—Sezione di Roma, piazzale Aldo Moro 2, 00185 Roma, Italy*
[21]*Istituto Nazionale di Fisica Nucleare, Sezione di Pavia, via Bassi 6, I-27100 Pavia, Italy*
[22]*Dipartimento di Fisica dell'Università di Roma "Tor Vergata", via della Ricerca Scientifica 1, I-00133 Roma, Italy*
[23]*Osservatorio Astrofisico di Torino dell'Istituto Nazionale di Astrofisica, via P. Giuria 1, I-10125 Torino, Italy*
[24]*Istituto Nazionale di Fisica Nucleare, Sezione di Torino, via P. Giuria 1, I-10125 Torino, Italy*
[25]*Dipartimento di Fisica dell'Università di Torino, via P. Giuria 1, I-10125 Torino, Italy*

(Received 8 February 2022; accepted 5 July 2022; published 26 July 2022)

*Corresponding author.
zhouxx@swjtu.edu.cn

The ARGO-YBJ detector, located at the Yangbajing Cosmic Ray Laboratory (4300 m a. s. l., Tibet, China), was a "full coverage" air shower array. The high altitude location and the frequent occurrence of thunderstorms, made ARGO-YBJ suitable to study the effects of atmospheric electric fields (AEF) on secondary cosmic rays. By analyzing the data of the ARGO-YBJ detector recorded during thunderstorms, significant variations of the rate of detected showers have been observed. During 20 thunderstorm episodes in 2012, the variations of the shower rates (both increases and decreases of amplitudes up to a few percent) are found to be correlated to the intensity and polarity of the AEF, and strongly dependent on the primary zenith angle. To understand the observed behavior, Monte Carlo simulations have been performed with CORSIKA and G4argo (a code based on GEANT4). We found that the data are well consistent with simulations, assuming the presence of a uniform electric field in a layer of thickness of 500 m in the atmosphere above the observation level. Due to the AEF accelerates/decelerates and deflects the secondary charged particles (mainly electrons and positrons) according to their charge, modifying the number and position of particles with energy exceeding the detector threshold. For the differences in electron and positron flux, spectrum, and lateral distribution, the AEF has an asymmetric effect on the shower particles, producing significant variations of the particle pattern on the ground, and, consequently, on the rate of detected showers, consistent with observations.

DOI: 10.1103/PhysRevD.106.022008

I. INTRODUCTION

Thunderstorms are common convective weather events, accompanied by intense lightning discharges, strong winds and rainstorms [1]. During thunderstorms, the strength of the electric field could be up to 1000 V/cm or even higher [2,3], and the polarity can change multiple times [4]. In such strong fields, the secondary charged particles of extensive air showers (EAS) could be accelerated or decelerated, causing the variations of the flux of secondary cosmic rays measured at the ground level.

In 1924, Wilson [5] introduced the concept of "runaway electrons," later developed by Gurevich *et al.* [6], and based on the idea that secondary electrons of EAS accelerated by the strong AEF gain energy exceeding that lost in ionization and bremsstrahlung. Due to the ionization of the air molecules, these electrons produce new electrons. Newborn free electrons are also accelerated by the field, giving rise to an avalanche process, i.e., a runaway breakdown (RB), now referred to as relativistic runaway electron avalanche (RREA) [7,8]. The RREA mechanism is thought to be responsible for thunderstorm ground enhancements (TGEs) that exceed by several times the background levels over timescales of seconds to tens of minutes [9–11]. Moreover, the source of terrestrial gamma-ray flashes (TGFs) [12–15], submillisecond gamma-ray emissions originated from bremsstrahlung by runaway electrons, is also identified to be the RREA process.

Dwyer [16] and Symbalisty *et al.* [17] investigated the field strength threshold to trigger the RREA process. The threshold $E_{\rm th}$ is found to be a function of the altitude, and can be expressed by $E_{\rm th} = E_0 e^{(-Z/8.4)}$, where Z is the height above sea level (in km), and the threshold at sea level E_0 is about 2800 V/cm. At $Z = 4.3$ km (the height of ARGO-YBJ observatory), $E_{\rm th} \approx 1680$ V/cm. This means that, to ensure the development of the RREA process, the strength of the electric field should be very large.

During thunderstorms, when the AEF is lower than the field strength threshold, several ground-based experiments reported frequent but modest (less than 10%) TGE events [18–20], and some of them observed a decrease of the soft component (electrons) flux [21]. These results show that the RREA mechanism alone cannot explain the variations of the ground cosmic ray flux during thunderstorms.

Significant increases of the rate of air showers during thunderstorms, lasting 10–20 min, have been observed by the EAS-TOP array, with amplitudes increasing with the shower size [22].

The dependence of ground cosmic ray flux variations on the polarity of AEF was discussed by [20,21,23–26]. Bartoli *et al.* [26] analyzed the scaler mode data of ARGO-YBJ and performed Monte Carlo simulations to investigate the development of electrons and positrons from EAS following the hypothesis introduced by Zhou *et al.* [27]. They concluded that the ground cosmic ray flux increases in negative fields and decreases in a certain range of positive fields. According to simulations, this behavior is due to the asymmetry in number and energy of electrons and positrons in EAS.

Chilingarian *et al.* [28–30] analyzed the energy spectra of gamma rays in the presence of AEF. They found an energy dependent additional flux of gamma rays. In thunderstorm fields, the spectra of gamma rays in the energy range 5–10 MeV can be expressed by an exponential function, then turns to a power law and extends up to 100 MeV. Yan *et al.* [31] investigated the field effects on the energy of ground cosmic rays, and found a significant enhancement of electrons and positrons in the energy region lower than 10 MeV and a small enhancement above 100 MeV.

During thunderstorms, the flux and energy of secondary particles of EAS could be significantly influenced. The time and positions of particles at the observation level will be affected as well. Axikegu *et al.* [32] studied the field effects on the lateral density of secondary positrons and electrons at the site of the ARGO-YBJ detector, and found that the lateral distribution becomes wider in the presence of electric fields.

In general, air shower arrays use trigger conditions based on the energy, arrival time, and position of the shower particles [33]. If these particle properties are affected by the electric fields, the detection and the reconstruction of showers will be affected as well. This will result in a variation of the shower rate and an altered reconstruction of shower parameters, as, for example, the arrival direction.

Compared with other ground-based experiments, ARGO-YBJ has two advantages to study the thunderstorm field effects on cosmic rays. On one hand, the detector was located at high-altitude, where thunderstorms are frequent and near to the shower maximum. On the other hand, the central full-coverage carpet makes the detector particularly suitable to observe the variations of particles properties in presence of electric fields.

The ARGO-YBJ detector was connected to two data acquisition systems (the scaler and shower operation modes), which worked independently. In scaler mode, the counting rate of each cluster was measured every 0.5 s [34]. In shower mode, the detector was triggered when at least 20 pads in the central carpet were fired within a time of 420 ns. Scaler data have been used to study the intensity variation of ground cosmic rays during thunderstorms, and the results have been reported by Bartoli *et al.* [26]. In this work we analyzed the correlation between the shower rates and the electric field, in particular studying the dependence of the rate variations on the zenith angle.

Comparing the data to the results of Monte Carlo simulations, we found a consistent explanation of the observed behavior.

II. THE ARGO-YBJ DETECTOR

The ARGO-YBJ detector, located at the Yangbajing Cosmic Ray Observatory (30°.11 N, 90°.53 E) in Tibet, China, at an altitude of 4300 m above sea level (corresponding to the atmospheric depth of 606 g/cm^2), was a "full coverage" (with a central carpet active area of ∼93%) air shower array, which ran in its full configuration from November 2007 to February 2013. The detector was composed of a single layer of resistive plate chambers (RPCs), operated in streamer mode, with a modular configuration. The basic module was a cluster of size 5.7×7.6 m^2, composed of 12 RPCs. Each RPC (of area 1.23×2.85 m^2) was read via 80 strips, logically organized in 10 pads (55.6×61.8 cm^2 each), providing a larger particle counting dynamic range [35]. The pads were the basic elements to define the space-time pattern of the shower, giving the position and the time of each detected hit. The detector was composed by a full coverage central carpet of area 78×74 m^2, made of 130 clusters, surrounded by a sampling guard ring of 23 clusters, which increased the effective area of the experiment and improved the resolution in the shower core position. The total area of the array was $\sim 110 \times 100$ m^2.

The ARGO-YBJ detector was connected to two independent data acquisition systems, corresponding to scaler and shower operation modes. In scaler mode [34,36], the counting rates of showers with a number of fired pads per cluster ≥ 1, 2, 3, and 4 (inside a time window of 150 ns) were recorded every 0.5 s. Scaler data are used to check the stability of the detector, to search for transient events like gamma-ray bursts (GRBs) in the GeV energy range [37,38], and to study the flux variation of ground cosmic rays during thunderstorms [26]. In shower mode [33], the detector was operated by requiring at least 20 fired pads within 420 ns on the central carpet detector. Within this time window there is a negligible chance that multiple cosmic rays hit the experiment causing a false trigger. The information on the arrival time and location of each particle was recorded to reconstruct the shower core position, the primary energy, and arrival direction. Shower data are used for gamma ray astronomy [39,40] and cosmic ray studies [41,42].

In order to study the field effects on cosmic rays, two EFMs (Electric Field Mills Boltek EFM-100) were mounted on the roof of the ARGO-YBJ building [26]. Data related to AEF (strength and polarity) were recorded every ∼20 s. The output of the mills was corrected to take into account their location (the edge of the roof causes a local enhancement of the electric field). The detailed methodology was introduced in Ref. [43]. After applying the correction factors, the field values of the two mills were found to be consistent within 10%, with a saturation value of ± 175 V/cm. The mean value of the two measurements is used in this work.

III. DATA SELECTION AND OBSERVATION RESULTS

A. Selection of thunderstorm episodes

To get a clearer correlation between the near-earth electric fields and the rate of shower detected by ARGO-YBJ, we only considered thunderstorm episodes with a saturated field ± 175 V/cm lasting at least for 4 min, or a field strength exceeding 90 V/cm for at least 8 min. The criteria are consistent with Ref. [26]. A total of 20 thunderstorm episodes met these criteria during the year 2012. Depending on the polarity of AEF, thunderstorm episodes can be classified into three types: negative-based field (signed as "−"), positive-based field (signed as "+"), and successions of positive and negative field (signed as "+/−"). Here, we define the positive field as the one that

TABLE I. 20 thunderstorm episodes detected at ARGO-YBJ Observatory in 2012.

Thunderstorm episodes	Thunderstorm types	Duration time (min)	Maximum field strength (V/cm)
120412	+	14	158
120427	+	17	≥175
120428-1	+/−	44	≥175
120428-2	+/−	42	158
120429	+/−	26	≥175
120528	−	27	≥175
120615	−	45	174
120619	−	31	130
120713	+	30	157
120714	+/−	55	≥175
120719	+/−	21	≥175
120723	+/−	26	≥175
120804	+/−	23	≥175
120808-1	+/−	26	124
120808-2	+/−	28	160
120819	+/−	34	155
120826	+/−	33	≥175
120914	+	18	116
120929	−	30	≥175
121010	+/−	45	≥175

accelerates the positrons downward in the direction of the Earth.

The information on the 20 thunderstorm events is listed in Table I. The thunderstorm name (shown in column 1) is based on the year, month, and day of its detection. If multiple thunderstorms are detected on the same day, an additional suffix "−1", "−2", … is added based on the sequence of their detection. The thunderstorm type, duration time, and the maximum field strength are shown in columns 2–4.

From Table I, it can be seen that 55% of thunderstorms occurred in summer (June, July, and August), while almost none in winter (December, January, and February). In addition, thunderstorm events characterized by a sequence of positive and negative fields are the majority. In terms of time duration, the thunderstorms lasted in average about 30 min. The electric field reached the saturation value in more than half of the episodes.

B. Rate variations of the shower events during thunderstorms

Figure 1(a) is an example of the AEF value and the shower rate variations (in percent) as a function of time (in 1 min bins) during a positive-based thunderstorm. The AEF disturbance lasted for 17 min, from 04:49 to 05:06 UT on April 27, 2012. During this interval, the absolute value of the AEF is saturated for 5 min. The event rate decreases in the positive field with an amplitude depending on the electric field intensity, with a maximum decrease of −2.3%.

A thunderstorm episode characterized by a sequence of positive and negative fields, reported in Fig. 1(b), occurred between 06:35 and 07:20 UT on October 10, 2012. The positive field lasted for 20 min, with a maximum strength of ∼130 V/cm. The negative field lasted for 25 min and saturated the instrument for 1 min. The decrease of the event rate in the positive field is consistent with the trend shown in Fig. 1(a). In the negative field, an increase occurred and the enhanced amplitude became larger with the electric field intensity, reaching ∼1.6% when the field intensity exceeded the saturation value. More thunderstorm episodes can be found in Supplemental Material [44].

Figure 2 shows the average event rate variations in the 20 selected thunderstorm events as a function of AEF (note that in this figure the points corresponding to the field ±185 V/cm include all the |AEF| ≥ 175 V/cm data). The variations strongly depend on the strength and polarity of AEF. In negative fields, the event rate increases with the AEF strength, with a maximum value of about 1.2% at the saturation value of −175 V/cm. In positive fields the rate

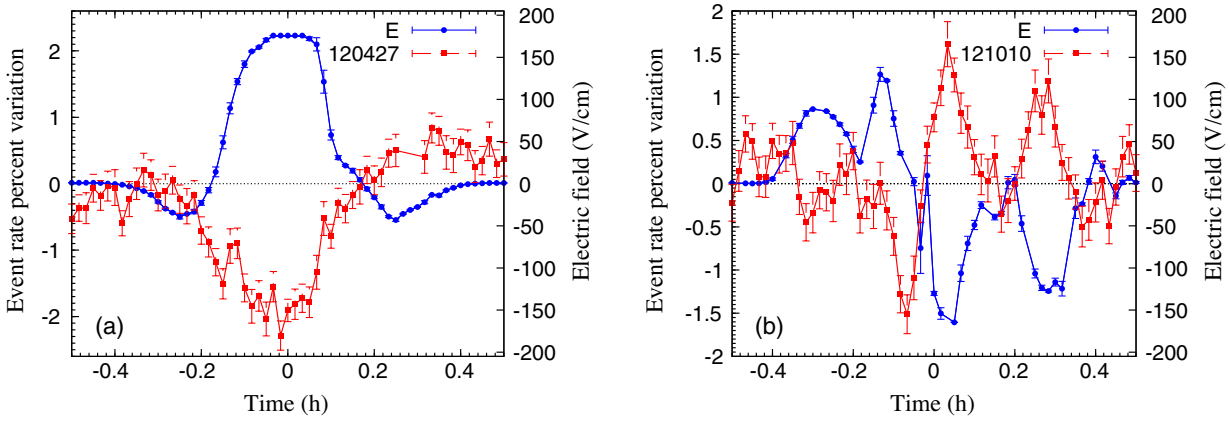

FIG. 1. Percent variation of the shower rate (red solid squares) and ground AEF intensity (blue dots) as a function of time (1 min/bin) during thunderstorm episodes 120427 (a) and 121010 (b).

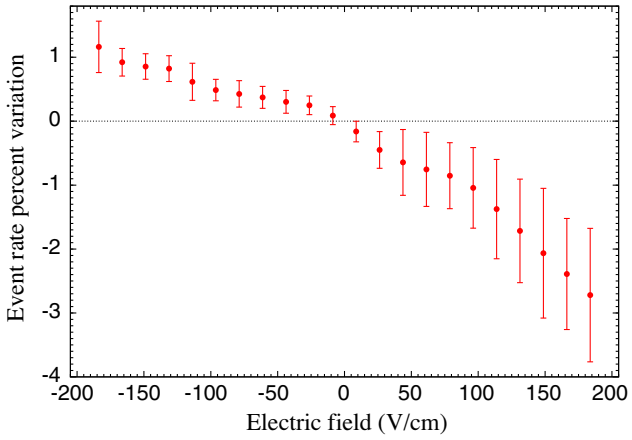

FIG. 2. Percent variation of the shower rate as a function of the ground AEF (averaged over 20 thunderstorm episodes). The error bars represent 1 standard deviation.

decreases, with a maximum declining amplitude of about −2.7%.

These trigger rate variations are due to a change of the number of hits on the detector carpet (one hit corresponds to a fired pad), caused by the presence of the electric field in the atmosphere. Figure 3(a) shows the percent variation of the hit number (nhit) distribution for two values of the AEF: −150 and +150 V/cm with respect to the distribution without AEF (note that in this figure the hit number of 120 includes all the nhit ≥ 120 data). In an AEF of −150 V/cm, if the number of hits is less than 32, the rate declines, with a maximum decrease of about −18%, otherwise the rate increases and the variation can be up to 3%. In an AEF of +150 V/cm, the rate decreases, with a maximum of about −20%. Figure 3(b) reports the variation of the integral distribution of the number of hits, for the same values of the field in Fig. 3(a). The rate increases in an AEF of −150 V/cm, with a maximum of about 1.5%. But the rate decreases in an AEF of +150 V/cm, with a maximum decrease of about −2%.

C. The zenith angle dependence of the rate variation

According to Zhou *et al.* [27] and Buitink *et al.* [45], the AEF has more effects on EAS charged particles with larger zenith angles. Here we report our results on the dependence of the rate variations on the reconstructed zenith angle. In order to limit statistical fluctuations, we divide the events in three large intervals of zenith angle: 0°–20°, 20°–40°, and 40°–60°.

Figure 4(a) shows the rate variations during a positive-based thunderstorm for different ranges of zenith angle. The AEF disturbance lasted for 23 min, from 17:18 to 17:41 UT on August 4, 2012. The event rates decrease in a positive-based field and the variation becomes larger with the zenith angle, reaching about −6.5% for the zenith angle interval 40°–60°. In Fig. 4(b), the AEF values and the rate variations for different zenith angle ranges are plotted during a negative-based thunderstorm. The AEF disturbance lasted for 27 min, from 19:05 to 19:32 UT on May 28, 2012. The negative field saturated the EFMs for 5 min. The rates of events with a zenith angle less than 40° increase and the variation becomes larger as the zenith angle decreases, reaching ∼3.8% for zenith angles in the range 0°–20°. At zenith angles higher than 40°, however, the event rates show a decrease that depends on the field intensity, with a maximum of −2.2%.

Figure 5 shows the average event rate variations for different zenith angle ranges as a function of AEF. The event rate variations are found to be correlated with the strength and polarity of the AEF and strongly dependent on the zenith angle. In negative fields, the rate of events with zenith angle less than 40° increases, and the variation depends on the AEF intensity and on the zenith angle, with a value of ∼2.2% for zenith angles in the interval 0–20°. For zenith angles in the range 40°–60°, the opposite situation occurs and the maximum decreasing amplitude exceeds −2.0%. In positive fields, the rate always decreases, and the variation increases with the AEF strength and the primary zenith angle, reaching about −6% for zenith angles in the range 40°–60°.

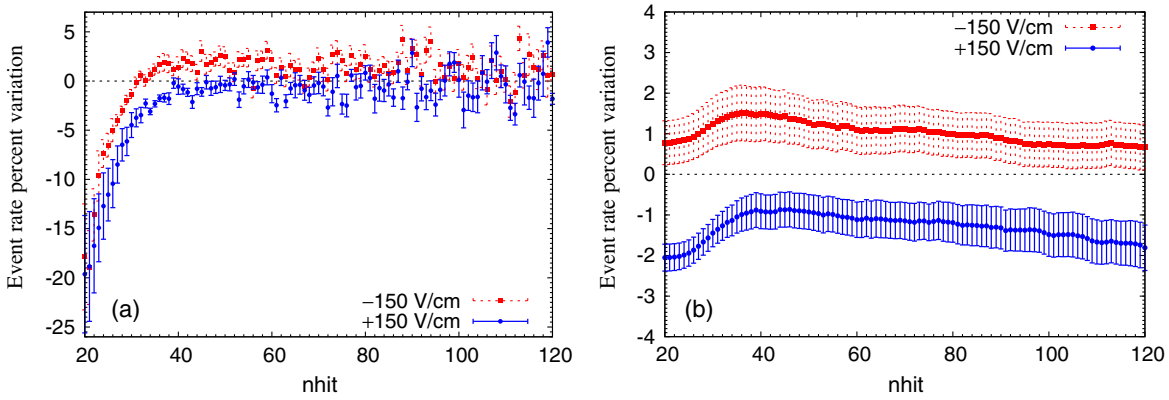

FIG. 3. (a) Variation of the hit number distribution in an electric field of −150 and −150 V/cm. (b) Integral distribution of the hit number variation. The error bars represent 1 standard deviation.

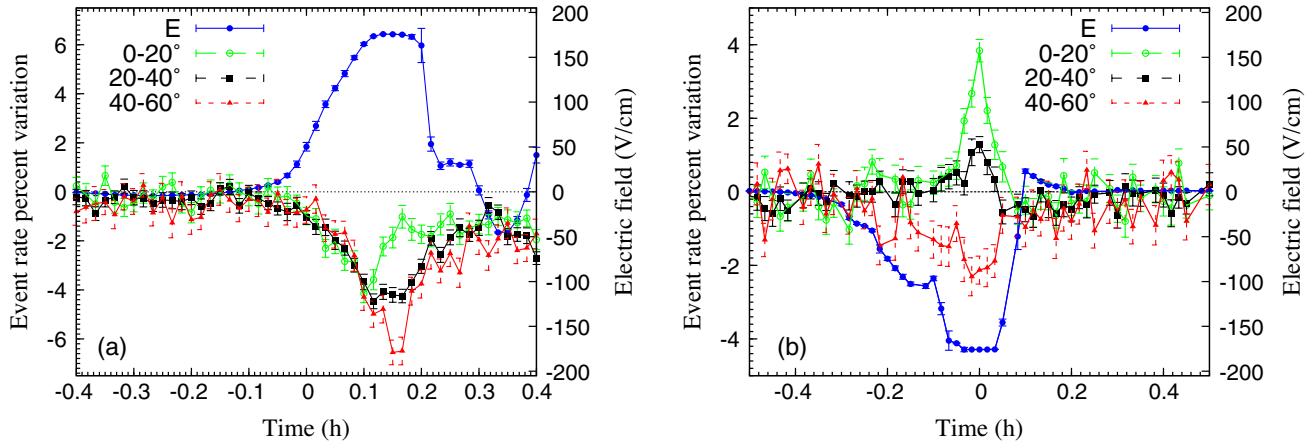

FIG. 4. Percent variations of shower rates for different zenith angle ranges and ground AEF intensity as a function of time (1 min/bin) during thunderstorm episodes 120804 (a) and 120528 (b).

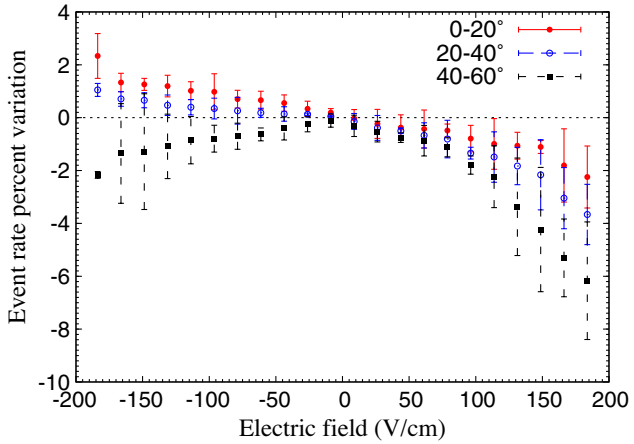

FIG. 5. Percent variations of shower rates for different zenith angle ranges as a function of the ground AEF (averaged over 20 thunderstorm episodes).

IV. SIMULATION RESULTS AD DISCUSSION

To understand the data recorded by the ARGO-YBJ detector in shower mode, simulations of the extensive air shower development and of the detector response have been performed. Some more simulation results can be found elsewhere [32].

The CORSIKA code (version 7.5700) [46] has been used to simulate air showers in the atmosphere. This code has been extended to account for the effect of atmospheric AEF on the transport of electrons and positrons. The hadronic interaction models selected are QGSJETII-04 for high energy events and GHEISHA in the low energy range. We assume proton primaries with arrival direction evenly distributed in the sky, with a zenith angle less than 60°. In view of the acceleration of the field, the energy cutoff for positrons and electrons is set to the lowest possible value of 50 keV, i.e., positrons and electrons with energy below this threshold are discarded from the simulation. The horizontal and vertical intensity of the geomagnetic field components used in simulations are $B_X = 34.1\ \mu$T and $B_Z = 36.2\ \mu$T, respectively [47]. According to the energy threshold of the ARGO-YBJ detector, a few hundreds of GeV in shower mode [33], the simulated primary particles are selected as protons with energy ranging from 100 to 10^6 GeV following a power-law function with a spectral index of -2.7.

The measurements of the thunderstorm electric fields are challenging to perform due to their violent nature [48]. To study the field effects, we use homogeneous ambient electric fields from -200 to 200 V/cm (lower than the threshold field strength to trigger RREA process at YBJ). This will certainly bring some deviations from a realistic situation. However, such simplification could easily clarify the effects of the thunderstorm electric fields on the secondary charged particles. In addition, Bartoli *et al.* [26] reported that the bottom of thunderclouds is typically a few hundred meters above the detector. Thus, we assume an AEF with a vertical direction, uniformly distributed in an atmospheric layer with a thickness of 500 m, extending from the ARGO-YBJ detector level (4300 m) up to 4800 m, corresponding to an atmospheric depth from 606 to 568 g/cm^2.

To simulate the ARGO-YBJ detector response, a specific software, G4argo [49], was developed in the framework of the GEANT4 package [50]. In these simulations, at least 20 fired pads in the central carpet of 130 clusters within a time window of 420 ns are required for a shower trigger. By using the official reconstruction procedures, the events meeting the trigger conditions are used to reconstruct the shower core and arrival direction. If the reconstructed core location is outside the array, the event is discarded, as for real data.

Figure 6 shows the rate variations of showers as a function of the AEF, according to the results of our simulations. We can see that the event rates decrease in positive fields and the variation becomes larger with the field intensity, exceeding -2.5% in a field of 200 V/cm. In negative fields, the opposite phenomenon occurs. Namely,

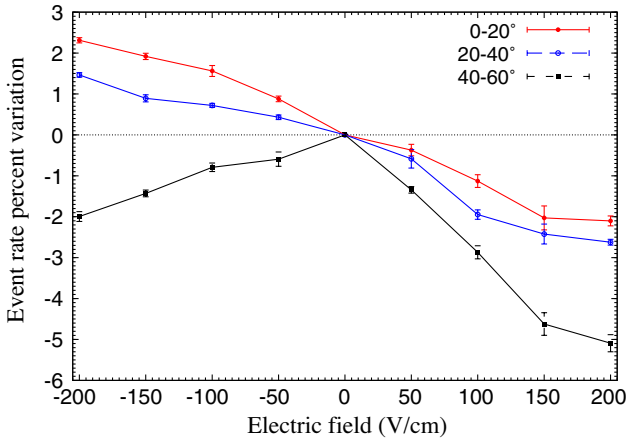

FIG. 6. Simulations: rate variations of shower events as a function of the electric field.

the event rates increase, and the variation is also depending on the AEF intensity, being up to 1.5% in a field of −200 V/cm. These trends are consistent with the data obtained by the ARGO-YBJ detector, shown in Fig. 2.

The effect shown in Fig. 6 can be easily understood. According to Refs. [26,27], the number of electrons in EASs exceeds that of positrons in EAS due to the asymmetry of production and absorption mechanisms. Also, the fraction of electrons with lower energies is higher than that of positrons. Thus, the effects of positive fields (accelerating positrons) on positrons are much smaller than that of negative fields (accelerating electrons) on electrons. During thunderstorms, the secondary positrons and electrons are accelerated or decelerated according to their charge, causing a significant variation of the number of particles with energy above the detector threshold, that is 2 MeV (details can be seen in Fig. 7 in Ref. [26]). As a consequence, the number of shower events satisfying the ARGO-YBJ trigger condition will also change. As a result, the shower rates increase in negative fields but decrease in positive fields and the variation amplitude is AEF dependent.

Figure 7 reports the event rate variations as a function of the number of hits on the detector carpet in an AEF of −150 and +150 V/cm, respectively. The experimental data are plotted to compare. It can be seen that the simulations are in agreement with the data. The large rate decrease of smaller showers in both polarization fields is probably due to the fact that less energetic showers (i.e., with a small number of hits) generally contain less energetic particles (as reported in our previous study [26]). The larger deflection effects of the electric field on low energy particles (in opposite direction for electrons and positrons) could cause a "loss" of particles from the detector area.

Figure 8 shows the percent change of events in different zenith angle ranges as a function of the electric field, obtained by simulations. The variations are correlated with the AEF polarity and zenith angle. In positive fields, the event rate decreases and the variation becomes larger with the zenith angle. It can be more than 5% for zenith angles in the range 40°–60° and an AEF of 200 V/cm. In negative fields, their behaviors are more complex. If the zenith angle is less than 40°, the rate increases, being larger for smaller zenith angles. The maximum value is about 2.3% for zenith angle 0–20° in a field of −200 V/cm. For zenith angles larger than 40°, however, the event rate decreases, and the amplitude is field intensity dependent, being about −2% in a field of −200 V/cm.

The comparison of the results of our simulations with experimental data is shown in Figs. 9. We can see that data and simulations are in very good agreement.

Combined with previous simulations [32,51], the ARGO-YBJ observations can be easily understood. In presence of an AEF, the lateral distribution of secondary charged particles becomes wider, and this effect increases with the zenith angle. For different distances from the shower core, the number of secondary particles may increase or decrease. Since in general the trigger conditions of an air shower detector require a certain number of detected particles in a given area, the variations of the particle number due to the electric field can alter the trigger

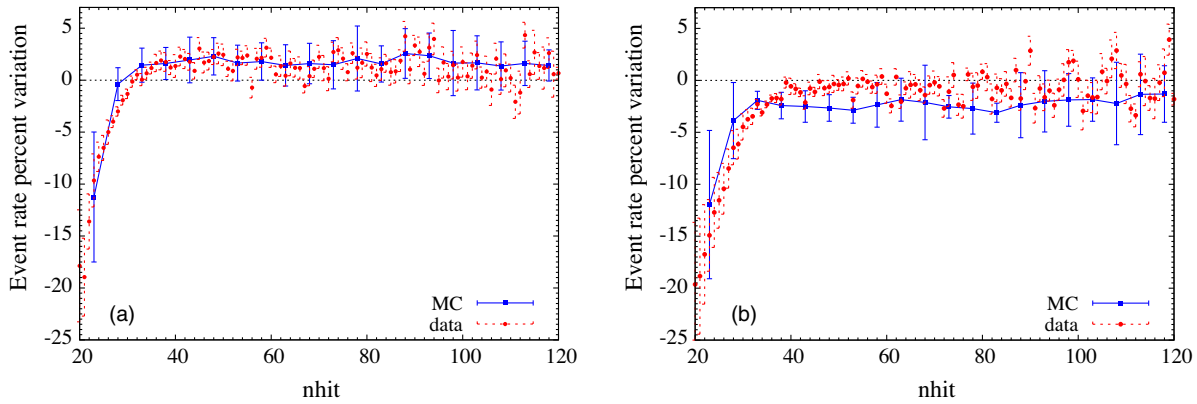

FIG. 7. Variation of the hit number distribution in an AEF of −150 (a) and +150 V/cm (b). Blue lines represent the simulations and red points represent the data.

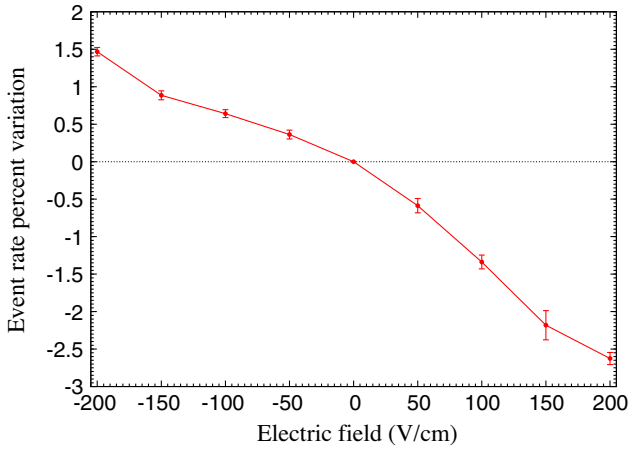

FIG. 8. Simulations: percent variations of shower events in different zenith angle ranges as a function of the AEF.

rate, in a way that depends on the position of the shower core and on the primary zenith angle.

In the ARGO-YBJ detector, the core position should be in the central carpet and the average distance of the detected particles from the shower core is about 40 m. From the integral change of particle number at distances from the shower core with less than 40 m (reported in Fig. 3 in Ref. [32]), in a negative field, an increase of the particle number occurs at small zenith angles and a decrease occurs at large zenith angles. However, it decreases in a positive field and the decreased amplitude becomes larger with zenith angle. This law is consistent with the observed data in ARGO-YBJ (shown in Fig. 9), showing that the observed trigger rate variations are actually due to the acceleration/deceleration and deflection effects of the electric field.

It has to be noted that for different detector sizes, with different mean distances of detected particles from the shower core, the dependence of event rate variations on the zenith angle in the presence of an AEF can be different, or even opposite. Figure 9 has showed the results observed in the ARGO-YBJ as an example of small detector size. When the size of the detector is the order of kilometers or infinite, for example, an opposite behavior occurs [32]. In the negative AEFs, the rate increases and the enhanced amplitude becomes larger with zenith angle. Positive fields produce a more complex behavior. For small AEF intensities, there is a clear rate decrease. Then, as AEF increases, the rate begins increasing and the variation amplitude increases with the zenith angle.

V. SUMMARY AND CONCLUSIONS

The variation of the detection rate of air showers by ARGO-YBJ during 20 thunderstorm episodes in 2012 has been studied. Significant rate variations (both increases and decreases) are observed in correlation with the atmospheric

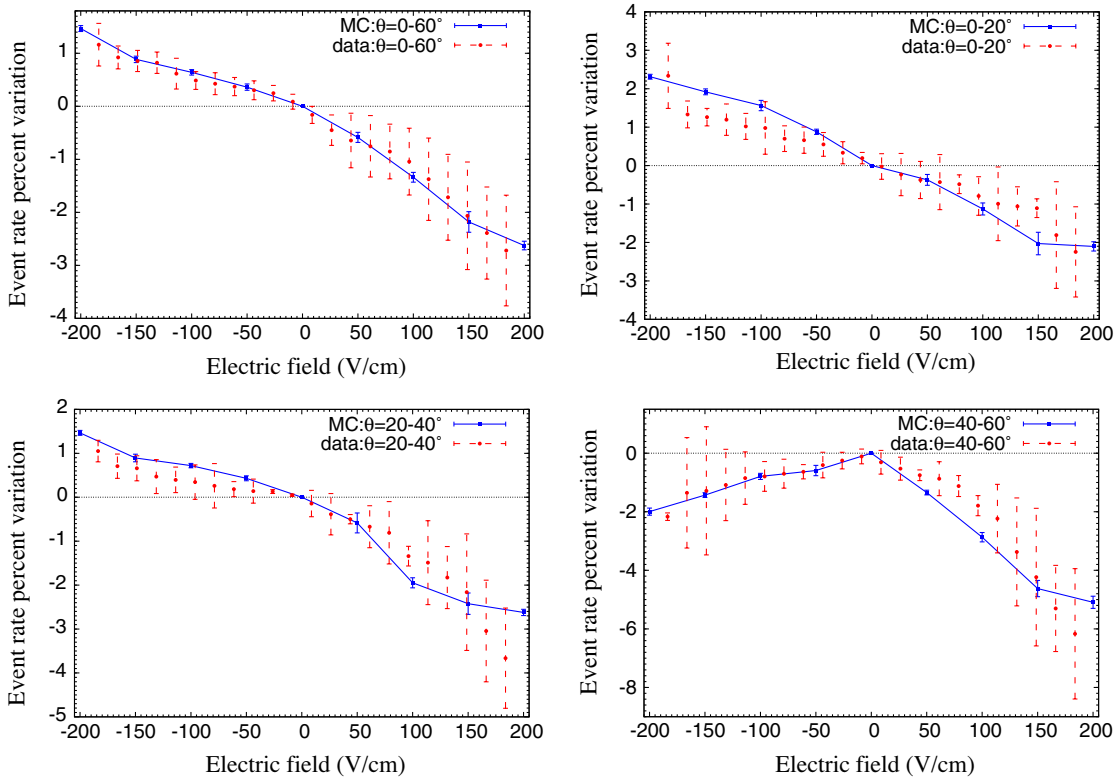

FIG. 9. Percent variations of shower rates as a function of the AEF strength for different zenith angle ranges. Red points represent the data and blue lines represent the simulations.

electric field strength. Generally, the detection rate decreases in positive fields (i.e., directed towards the ground), and mostly increases in negative fields. The variation amplitude is not only correlated with the strength and polarity of the electric field, but also highly dependent on the primary zenith angle.

To study this dependence we divided the events into three groups according to the zenith angle: 0°–20°, 20°–40° and 40°–60°. We found that in positive electric fields the detection rate always decreases and the amplitude of the variation increases with the zenith angle, reaching −5% in the zenith angle range 40°–60°. In negative electric fields, the rate decreases for zenith angles 40°–60°, but increases for smaller angles, the variation becoming larger as the angle decreases. The maximum rate variation is 2.3% in the range 0–20°.

During the thunderstorm episodes considered here, the AEFs strengths are found to be less than the threshold field able to trigger RREA process, that in our case cannot be considered responsible for the observed rate variations. On the other hand, our data can be fully understood considering the acceleration/deceleration and deflection effects of the electric field on electrons and positrons of air showers. Electrons and positrons act in opposite ways under the effect of an electric field. The different properties of electrons and positrons in a shower, i.e., the total number, the energy spectrum and lateral distribution, produce a complex variation of the shower morphology under the effect of the field, resulting in an increase or decrease of the particle number at different distances from the shower core.

For any given shower, the variations of the spectrum and lateral distribution of particles will affect both the number of particles and their position on the ground. Since the ARGO-YBJ trigger condition for showers is defined by the number of hits in the central carpet, the modification of the shower pattern will result in a variation of the trigger rate.

The Monte Carlo simulation that we performed assuming a uniform electric field in a layer of thickness 500 m above the detection level, can describe all the observations, founding an excellent agreement with data, in terms of the amplitude and sign of the detection rate variations, for different strength and polarity of the field (up to about ± 200 V/cm) and for different zenith angles of the primary cosmic ray arrival direction.

The Large High Altitude Air Shower Observatory has been constructed at Haizi Mountain (4410 m a. s. l.) in China. Analyzing the data of shower modes [52] and scaler modes [53], the correlations between the thunderstorm electric fields and cosmic ray variations will be studied in more detail.

ACKNOWLEDGMENTS

This work is supported in China by the National Natural Science Foundation of China (NSFC) under the Grants No. U2031101 and No. 11475141, the National Key R&D Program of China under the Grant No. 2018YFA0404201, the Chinese Academy of Science (CAS), the Key Laboratory of Particle Astrophysics, Institute of High Energy Physics (IHEP), and in Italy by the Istituto Nazionale di Fisica Nucleare (INFN). We also acknowledge the essential support of W. Y. Chen, G. Yang, X. F. Yuan, C. Y. Zhao, R. Assiro, B. Biondo, S. Bricola, F. Budano, A. Corvaglia, B. D'Aquino, R. Esposito, A. Innocente, A. Mangano, E. Pastori, C. Pinto, E. Reali, F. Taurino, and A. Zerbini in the installation, debugging, and maintenance of the detector.

[1] X. S. Qie *et al.*, Understanding the dynamical microphysical electrical processes associated with severe thunderstorms over the Beijing metropolitan region, Sci. China Earth Sci. **64**, 10 (2021).
[2] T. C. Marshall *et al.*, Observed electric fields associated with lightning initiation, Geophys. Res. Lett. **32**, L03813 (2005).
[3] A. Chilingarian, T. Karapetyan, M. Zazyan, G. Hovsepyan, B. Sargsyan, N. Nikolova, H. Angelov, J. Chum, and R. Langer, Maximum strength of the atmospheric electric field, Phys. Rev. D **103**, 043021 (2021).
[4] J. F. Wang, X. S. Qie, H. Lu, J. L. Zhang, X. X. Yu, and F. Shi, Effect of thunderstorm electric field on intensity of cosmic ray muons, Acta Phys. Sin. **61**, 159202 (2012).
[5] R. C. T. Wilson, The electric field of a thundercloud and some of its effects, Proc. Phys. Soc. London **37**, 32D (1924).
[6] A. V. Gurevich, G. M. Milikh, and R. Roussel-Dupre, Runaway electron mechanism of air breakdown and preconditioning during a thunderstorm, Phys. Lett. A **165**, 463 (1992).
[7] L. P. Babich, I. M. Kutsyk, E. N. Donskoy, and A. Y. Kudryavtsev, New data on space and time scales of relativistic runaway electron avalanche for thunderstorm environment: Monte Carlo calculations, Phys. Lett. A **245**, 460 (1998).
[8] J. R. Dwyer, The relativistic feedback discharge model of terrestrial gamma ray flashes, J. Geophys. Res. Space Phys. **117**, A02308 (2012).
[9] J. Chum, R. Langer, J. Baše, M. Kollárik, I. Strhárský, G. Diendorfer, and J. Rusz, Significant enhancements of secondary cosmic rays and electric field at the high mountain peak of Lomnický Štít in High Tatras during thunderstorms, Earth Planets Space **72**, 28 (2020).
[10] A. Chilingarian, H. Mkrtchyan, G. Karapetyan, S. Chilingaryan, B. Sargsyan, and A. Arestakesyan, Catalog

of 2017 Thunderstorm Ground Enhancement (TGE) events observed on Aragats, Sci. Rep. **9**, 6253 (2019).
[11] A. Chilingarian, G. Hovsepyan, T. Karapetyan, G. Karapetyan, and B. Sargsyan, Structure of thunderstorm ground enhancements, Phys. Rev. D **101**, 122004 (2020).
[12] G. J. Fishman *et al.*, Discovery of intense gamma-ray flashes of atmospheric origin, Science **264**, 1313 (1994).
[13] D. M. Smith, L. I. Lopez, R. P. Lin, and C. P. Barrington-Leigh, Terrestrial gamma-ray flashes observed up to 20 MeV, Science **307**, 1085 (2005).
[14] Y. Wada, T. Enoto, K. Nakazawa, Y. Furuta, T. Yuasa, Y. Nakamura, T. Morimoto, T. Matsumoto, K. Makishima, and H. Tsuchiya, Downward Terrestrial Gamma-Ray Flash Observed in a Winter Thunderstorm, Phys. Rev. Lett. **123**, 061103 (2019).
[15] N. Torsten *et al.*, A terrestrial gamma-ray flash and ionospheric ultraviolet emissions powered by lightning, Science **367**, 183 (2020).
[16] J. R. Dwyer, A fundamental limit on electric fields in air, Geophys. Res. Lett. **30**, 2055 (2003).
[17] E. M. D. Symbalisty, R. A. Roussel-Dupre, and V. A. Yukhimuk, Finite volume solution of the relativistic Boltzmann equation for electron avalanche studies, IEEE Trans. Plasma Sci. **26**, 1575 (1998).
[18] A. Chilingarian, T. Karapetan, and L. Melkumyan, Statistical analysis of the Thunderstorm Ground Enhancements (TGEs) detected on Mt. Aragats, Adv. Space Res. **52**, 1178 (2013).
[19] J. R. Dwyer and M. A. Uman, The physics of lightning, Phys. Rep. **534**, 147 (2014).
[20] K. Kudela, J. Chum, M. Kollárik, R. Langer, I. Strhárský, and J. Baše, Correlations between secondary cosmic ray rates and strong electric fields at Lomnický štít, J. Geophys. Res. **122**, 10,700 (2017).
[21] V. V. Alexeenko, N. S. Khaerdinov, A. S. Lidvansky, and V. B. Petkov, Transient variations of secondary cosmic rays due to atmospheric electric field and evidence for pre-lightning particle acceleration, Phys. Lett. A **301**, 299 (2002).
[22] S. Vernetto for EAS-TOP Collaboration, The EAS counting rate during thunderstorms, in, *Proceedings of 27th ICRC, Copernicus Gesellschaft, Hamburg, Germany* (2001), Vol. 10, p. 4165.
[23] A. S. Lidvansky, The effect of the electric field of the atmosphere on cosmic rays, J. Phys. G **29**, 925 (2003);
[24] N. S. Khaerdinov, A. S. Lidvansky, and V. B. Petkov, Electric field of thunderclouds and cosmic rays: Evidence for acceleration of particles (runaway electrons), Atmos. Res. **76**, 346 (2005);
[25] B. Hariharan *et al.* (GRAPES-3 Collaboration), Measurement of the Electrical Properties of a Thundercloud Through Muon Imaging by the GRAPES-3 Experiment, Phys. Rev. Lett. **122**, 105101 (2019).
[26] B. Bartoli *et al.* (ARGO-YBJ Collaboration), Observation of the thunderstorm-related ground cosmic ray flux variations by ARGO-YBJ, Phys. Rev. D **97**, 042001 (2018).
[27] X. X. Zhou, X. J. Wang, D. H. Huang, and H. Y. Jia, Effect of near-earth thunderstorms electric field on the intensity of ground cosmic ray positrons/electrons in Tibet, Astropart. Phys. **84**, 107 (2016).
[28] A. Chilingarian, B. Mailyan, and L. Vanyan, Recovering of the energy spectra of electrons and gamma rays coming from the thunderclouds, Atmos. Res. **114–115**, 1 (2012).
[29] A. Chilingarian, G. Hovsepyan, and L. Vanyan, On the origin of the particle fluxes from the thunderclouds: Energy spectra analysis, Europhys. Lett. **106**, 59001 (2014).
[30] A. Chilingarian, G. Hovsepya, E. Svechnikova, and M. Zazyan, Electrical structure of the thundercloud and operation of the electron accelerator inside it, Astropart. Phys. **132**, 102615 (2021).
[31] R. R. Yan, D. H. Huang, B. Zhao, K. G. Axi, and X. X. Zhou, Effect of thunderstorm electric field on the cosmic ray secondary particle energy at LHAASO, China Astron. Astrophys. **44**, 146 (2020).
[32] K. G. Axi, X. X. Zhou, Z. C. Huang, and D. H. Huang, Intensity variations of showers with different zenith angle ranges during thunderstorms, Astrophys. Space Sci. **367**, 30 (2022).
[33] B. Bartoli *et al.* (ARGO-YBJ Collaboration), Search for gamma-ray bursts with the ARGO-YBJ detector in shower mode, Astrophys. J. **842**, 31 (2017).
[34] G. Aielli *et al.* (ARGO-YBJ Collaboration), Scaler mode technique for the ARGO-YBJ detector, Astropart. Phys. **30**, 85 (2008).
[35] C. Bicci *et al.* (ARGO-YBJ Collaboration), Results from the ARGO-YBJ test experiment, Astropart. Phys. **17**, 151 (2002).
[36] G. Aielli *et al.* (ARGO-YBJ Collaboration), Search for gamma ray bursts with the ARGO-YBJ detector in scaler mode, Astrophys. J. **699**, 1281 (2009).
[37] S. Vernetto, Detection of gamma-ray bursts in the 1 GeV–1 TeV energy range by ground-based experiments, Astropart. Phys. **13**, 75 (2000).
[38] B. Bartoli *et al.* (ARGO-YBJ Collaboration), Search for GeV gamma-ray bursts with the ARGO-YBJ detector: Summary of eight years of observations, Astrophys. J. **794**, 82 (2014).
[39] B. Bartoli *et al.* (ARGO-YBJ Collaboration), TeV gamma ray survey of the northern sky using the ARGO-YBJ detector, Astrophys. J. **779**, 27 (2013).
[40] B. Bartoli *et al.* (ARGO-YBJ Collaboration), Study of the diffuse gamma-ray emission from the Galactic plane with ARGO-YBJ, Astrophys. J. **806**, 20 (2015).
[41] B. Bartoli *et al.* (ARGO-YBJ Collaboration), Cosmic ray proton plus helium energy spectrum measured by the ARGO-YBJ experiment in the energy range 3–300 TeV, Phys. Rev. D **91**, 112017 (2015).
[42] B. Bartoli *et al.* (ARGO-YBJ Collaboration), Knee of the cosmic hydrogen and helium spectrum below 1 PeV measured by ARGO-YBJ and a Cherenkov telescope of LHAASO, Phys. Rev. D **92**, 092005 (2015).
[43] F. D. Alessandro, The use of "field intensification factors" in calculations for lightning protection of structures, J. Electrost. **58**, 17 (2003).
[44] See Supplemental Material at http://link.aps.org/supplemental/10.1103/PhysRevD.106.022008 for cosmic ray shower rate variations of 20 selected thunderstorms.
[45] S. Buitink, T. Huege, H. Falcke, D. Heck, and J. Kuijpers, Monte Carlo simulations of air showers in atmospheric electric fields, Astropart. Phys. **33**, 1 (2010).

[46] D. Heck, J. Knapp, J. N. Capdevielle, G. Schatz, and T. Thouw, CORSIKA: A Monte Carlo code to simulate extensive air showers, Report No. FZKA-6019, 1998, https://www.ikp.kit.edu/corsika/70.php.

[47] NOAA national centers for environmental information, Magnetic Field Calculators: IGRF model (1590–2024), https://www.ngdc.noaa.gov/geomag/calculators/magcalc.shtml#igrfwmm.

[48] T. Logan, Anomalous lightning behavior during the 26–27 August 2007 Northern Great Plains severe weather event, J. Geophys. Res. **123**, 1771 (2018).

[49] Y. Q. Guo *et al.*, ARGO-YBJ detector simulation using GEANT4, Chin. Phys. C **34**, 555 (2010).

[50] S. Agostinelli *et al.* (GEANT4 Collaboration), GEANT4—A simulation toolkit, Nucl. Instrum. Methods Phys. Res., Sect. A **506**, 250 (2003).

[51] T. N. G. Trinh, O. Scholten, S. Buitink, K. D. de Vries, P. Mitra, T. Phong Nguyen, and D. T. Si, Determining atmospheric electric fields using MGMR3D, Phys. Rev. D **105**, 063027 (2022).

[52] F. Aharonian *et al.* (LHAASO Collaboration), Observation of the Crab Nebula with LHAASO-KM2A—A performance study, Chin. Phys. C **45**, 025002 (2021).

[53] Z. C. Huang, X. X. Zhou, D. H. Huang *et al.*, Simulation study of scaler mode at large high altitude air shower observatory, Acta Phys. Sin. **70**, 199301 (2021).